NETWORKS AND HETEROGENEOUS MEDIA
©American Institute of Mathematical Sciences
Volume **11**, Number **1**, March **2016**
doi:10.3934/nhm.2016.11.1
pp. **1–27**

A COMBINED FINITE VOLUME - FINITE ELEMENT SCHEME FOR A DISPERSIVE SHALLOW WATER SYSTEM

Nora Aïssiouene, Marie-Odile Bristeau
Edwige Godlewski and Jacques Sainte-Marie

Inria, EPC ANGE, 2 rue Simone Iff
F75012 Paris, France
CEREMA, EPC ANGE, 134 rue de Beauvais
F-60280 Margny-Les-Compiegne, France
Sorbonne Universités
UPMC Univ Paris 06
UMR 7598, Laboratoire Jacques-Louis Lions
F-75005, Paris, France
CNRS, UMR 7598, Laboratoire Jacques-Louis Lions
F-75005, Paris, France

Abstract. We propose a variational framework for the resolution of a non-hydrostatic Saint-Venant type model with bottom topography. This model is a shallow water type approximation of the incompressible Euler system with free surface and slightly differs from the Green-Nagdhi model, see [13] for more details about the model derivation.

The numerical approximation relies on a prediction-correction type scheme initially introduced by Chorin-Temam [17] to treat the incompressibility in the Navier-Stokes equations. The hyperbolic part of the system is approximated using a kinetic finite volume solver and the correction step implies to solve a mixed problem where the velocity and the pressure are defined in compatible finite element spaces.

The resolution of the incompressibility constraint leads to an elliptic problem involving the non-hydrostatic part of the pressure. This step uses a variational formulation of a shallow water version of the incompressibility condition.

Several numerical experiments are performed to confirm the relevance of our approach.

1. **Introduction.** Starting from the incompressible Euler or Navier-Stokes system, the hydrostatic assumption consists in neglecting the vertical acceleration of the fluid. More precisely the momentum along the vertical axis of the Euler equation

$$\frac{\partial w}{\partial t} + u\frac{\partial w}{\partial x} + w\frac{\partial w}{\partial z} + \frac{\partial p}{\partial z} = -g,$$

reduces in the hydrostatic context to

$$\frac{\partial p}{\partial z} = -g, \tag{1}$$

where p is the pressure, g is the gravitational constant, and u (resp. w) is the horizontal (resp. vertical) component of the fluid velocity.

2010 *Mathematics Subject Classification.* Primary: 65M06, 65M60, 76M10; Secondary: 76B15.
Key words and phrases. Projection method, non-hydrostatic, Navier-Stokes, Euler, free surface, depth-averaged Euler system, dispersive.

* Corresponding author: Nora Aïssiouene nora.aissiouene@inria.fr.

Such an assumption produces important consequences over the structure and complexity of the model. Indeed, Eq. (1) implies that the pressure p is no longer the Lagrange multiplier of the incompressibility constraint and p can be expressed, for free surface flows, as a function of the water depth of the fluid. Therefore, the hydrostatic assumption implies that the resulting model, even though it describes an incompressible fluid, has common features with models arising in compressible fluid mechanics.

In geophysical problems, the hydrostatic assumption coupled with a shallow water type description of the flow is often used. Unfortunately, these models do not represent phenomena containing dispersive effects for which the non-hydrostatic contribution cannot be neglected. More complex models have to be considered to take into account this kind of phenomena, together with numerical methods able to discretize the high order derivative terms coming from the dispersive effects. Many shallow water type dispersive models have been proposed such as KdV, Boussinesq, Green-Naghdi, see [24, 15, 6, 32, 33, 7, 16, 29, 2, 3, 14]. The modeling of the non-hydrostatic effects for shallow water flows does not raise insuperable difficulties but their discretization is more tricky. Numerical techniques for the approximation of these models have been recently proposed [16, 12, 30].

The depth-averaged Euler model studied in the present paper has been derived and studied in [13]. A numerical approximation based on a prediction-correction strategy [17] is described in [1], where the discretization of the elliptic part arising from the non-hydrostatic terms is carried out in a finite difference framework. It is worth noticing that the numerical scheme given in [1] is endowed with robustness and stability properties such as positivity, well-balancing, discrete entropy and wet/dry interfaces treatment.

Since the derivation in a 2d context of the model proposed in [13] does not raise difficulty, the objective is to have a numerical method that can be easily extended to the two dimensional problem. In [1], a finite volume method is used for the prediction part, while a finite difference method is applied for the projection part, which is not easy to apply on an unstructured grid in the 2d framework. The main contents of this paper is the derivation and validation of the correction step in a variational framework allowing a finite element approximation. The results depicted in this paper pave the way for a discretization of the 2d model on an unstructured mesh.

Notice that the non-hydrostatic model we consider slightly differs from the well-known Green-Naghdi model [24], see remarks 1,6 and [13] for more details.

Let $\Omega \subset \mathbb{R}$, be a 1d domain (an interval) and $\Gamma = \Gamma_{in} \cup \Gamma_{out}$ its boundary (see figure 1). The non-hydrostatic depth-averaged Euler model derived in [13, 1] reads

$$\frac{\partial H}{\partial t} + \frac{\partial H\overline{u}}{\partial x} = 0, \tag{2}$$

$$\frac{\partial H\overline{u}}{\partial t} + \frac{\partial}{\partial x}(H\overline{u}^2 + g\frac{H^2}{2} + H\overline{p}_{nh}) = -(gH + 2\overline{p}_{nh})\frac{\partial z_b}{\partial x}, \tag{3}$$

$$\frac{\partial H\overline{w}}{\partial t} + \frac{\partial H\overline{w}\overline{u}}{\partial x} = 2\overline{p}_{nh}, \tag{4}$$

$$\frac{\partial H\bar{u}}{\partial x} - \bar{u}\frac{\partial(H + 2z_b)}{\partial x} + 2\bar{w} = 0, \tag{5}$$

where H is the water depth, z_b is the topography and p_{nh} is the non-hydrostatic part of the pressure. The variables denoted with a bar recall that this model is

obtained performing an average along the water depth of the incompressible Euler system with free surface. The velocity field is denoted $\bar{\mathbf{u}} = (\bar{u}, \bar{w})^t$ with $\bar{u}$ (resp. $\bar{w}$) the horizontal (resp. vertical) component.

We denote $\eta = H + z_b$ the free surface of the fluid. In addition, we give the following notation

$$\mathbf{n} = \begin{pmatrix} n \\ 0 \end{pmatrix}, \tag{6}$$

with n the unit outward normal vector at Γ (in 1d, $n = \pm 1$), $\mathbf{n}$ represents the unit outward normal vector of the domain covered by the fluid, namely $\Omega \times [z_b, \eta]$. We also consider the gradient operator

$$\nabla_0 = \begin{pmatrix} \frac{\partial}{\partial x} \\ 0 \end{pmatrix}. \tag{7}$$

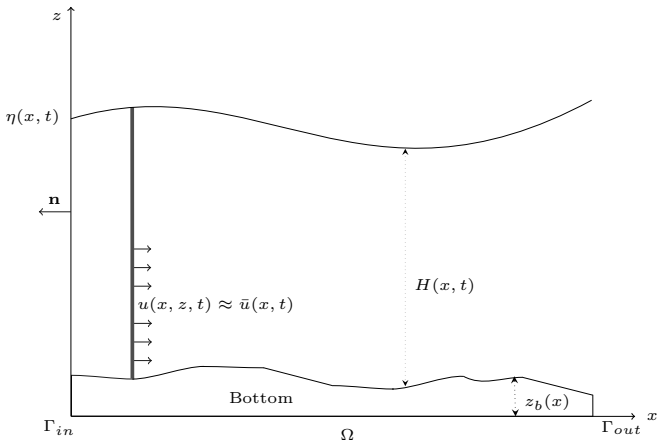

FIGURE 1. Notations and domain definition.

Moreover, the smooth solutions of the system (2)-(5) satisfy an energy conservation law, namely

$$\frac{\partial \bar{E}}{\partial t} + \frac{\partial}{\partial x}\left(\bar{u}\left(\bar{E} + \frac{g}{2}H^2 + H\bar{p}_{nh}\right)\right) = 0, \tag{8}$$

with

$$\bar{E} = \frac{H\left(\bar{u}^2 + \bar{w}^2\right)}{2} + \frac{gH\left(\eta + z_b\right)}{2}. \tag{9}$$

Equation (5) represents a shallow water version of the divergence free constraint, for which the non hydrostatic pressure $\bar{p}_{nh}$ plays the role of a Lagrange multiplier. The reader can refer to [13] for more details. Notice that considering $\bar{p}_{nh} = 0$ and neglecting (4), the system (2)-(3),(5) reduces to the classical Saint-Venant system.

The paper is organized as follows. First we give a rewriting of the model and we present the prediction-correction method, the main part being the variational formulation of the correction part. Then in Section 3, we detail the numerical approximation. Finally, in Section 4.1 and 5, numerical simulations validating the proposed discretization techniques are presented.

2. **The projection scheme for the non-hydrostatic model.** Projection methods have been introduced by A. Chorin and R. Temam [35] in order to compute the pressure for incompressible Navier-Stokes equations. These methods, based on a time splitting scheme, have been widely studied and applied to treat the incompressibility constraint (see [27, 37, 36]). We develop below an analogue of this method for shallow water flow. In order to describe the fractional time step method we use, we propose a rewritting of the model (2)-(5).

2.1. **A rewritting.** Let us introduce the two operators ∇_{sw} and div_{sw} defined by

$$\nabla_{sw} f = \begin{pmatrix} H\frac{\partial f}{\partial x} + f\frac{\partial (H+2z_b)}{\partial x} \\ -2f \end{pmatrix}, \tag{10}$$

$$\mathrm{div}_{sw}(\mathbf{v}) = \frac{\partial H v_1}{\partial x} - v_1 \frac{\partial (H+2z_b)}{\partial x} + 2v_2, \tag{11}$$

with $\mathbf{v} = (v_1, v_2)^t$. We assume for a while that f and $\mathbf{v}$ are smooth enough. The shallow water form of the divergence operator div_{sw} (resp. of the gradient operator ∇_{sw}) corresponds to a depth-averaged version of the divergence (resp. gradient) appearing in the incompressible Euler and Navier-Stokes equations. Notice that the two operators ∇_{sw} , div_{sw} defined by (10)-(11) are H and z_b dependent and we assume that H and z_b are sufficiently smooth functions. One can check that these operators verify the fundamental duality relation

$$\int_\Omega \mathrm{div}_{sw}(\mathbf{v}) f \, dx = -\int_\Omega \nabla_{sw} f \cdot \mathbf{v} \, dx + [H v_1 f]_\Gamma . \tag{12}$$

These definitions allow to rewrite the model (2)-(5) as

$$\frac{\partial H}{\partial t} + \frac{\partial H\bar{u}}{\partial x} = 0, \tag{13}$$

$$\frac{\partial H\bar{\mathbf{u}}}{\partial t} + \frac{\partial}{\partial x}(\overline{u} H \overline{\mathbf{u}}) + \nabla_0 \left(\frac{g}{2} H^2\right) + \nabla_{sw} \bar{p}_{nh} = -gH\nabla_0 z_b, \tag{14}$$

$$\mathrm{div}_{sw}(\bar{\mathbf{u}}) = 0, \tag{15}$$

with ∇_0 defined by (7).

Remark 1. It has been established in [13] that, when $z_b = 0$, the Green Naghdi model can be written in the form (2)-(4) with a different coefficient in the right hand side of the equation (4), which is replaced by

$$\frac{\partial H\overline{w}}{\partial t} + \frac{\partial H\overline{wu}}{\partial x} = \frac{3}{2}\overline{p}_{nh}. \tag{16}$$

So, if we try to write the Green-Naghdi model in the form (13)-(15), the duality relation (12) is no longer satisfied. Therefore the energy balance will also differ by one coefficient and the stability results established in [1] and based on the energy balance does not apply to the Green-Naghdi model.

The system (13)-(15) can be written in the compact form

$$\frac{\partial X}{\partial t} + \frac{\partial}{\partial x} F(X) + R_{nh} = S(X), \tag{17}$$

$$\mathrm{div}_{sw}(\bar{\mathbf{u}}) = 0, \tag{18}$$

where we denote

$$X = \begin{pmatrix} H \\ H\bar{u} \\ H\bar{w} \end{pmatrix}, \qquad F(X) = \begin{pmatrix} H\bar{u} \\ H\bar{u}^2 + \frac{g}{2}H^2 \\ H\bar{u}\bar{w} \end{pmatrix}, \tag{19}$$

and

$$R_{nh} = \begin{pmatrix} 0 \\ \nabla_{sw}\,\bar{p}_{nh} \end{pmatrix}, \qquad S(X) = \begin{pmatrix} 0 \\ -gH\nabla_0 z_b \end{pmatrix}. \tag{20}$$

Let be given time steps Δt^n and note $t^n = \sum_{k\leq n} \Delta t^k$. As detailed in [1], the projection scheme for system (17)-(18) consists in the following time splitting

$$\begin{aligned} X^{n+1/2} &= X^n - \Delta t^n \frac{\partial}{\partial x} F(X^n) + \Delta t^n\, S(X^n), && (21)\\ X^{n+1} &= X^{n+1/2} - \Delta t^n\, R_{nh}^{n+1}, && (22)\\ \mathrm{div}_{sw}\,\bar{\mathbf{u}}^{n+1} &= 0, && (23) \end{aligned}$$

with $\bar{\mathbf{u}}^{n+1} = \left(\frac{(H\bar{u})^{n+1}}{H^{n+1}}, \frac{(H\bar{w})^{n+1}}{H^{n+1}}\right)^t$.

The first two equations of (21) consist in the classical Saint-Venant system with topography and the third equation is an advection equation for the quantity $H\bar{w}$. Equations (22)-(23) describe the correction step allowing to determine the non hydrostatic part of the pressure p_{nh}^{n+1} and hence giving the corrected state X^{n+1}. The numerical resolution of (21) – especially the first two equations – has received an extensive coverage and efficient and robust numerical techniques exist, mainly based on finite volume approach, see [9, 5]. The derivation of a robust and efficient numerical technique for the resolution of the correction step (22)-(23) is the key point. A strategy based on a finite difference approach has been proposed, studied and validated in [1]. Unfortunately, the finite difference framework does not allow to tackle situations with unstructured meshes in 2 or 3 dimensions. It is the key point of this paper to propose a variational formulation of the correction step coupled with a finite volume discretization of the prediction step.

2.2. **The correction step.** In this part, we consider we have at our disposal a space discretization of Eq. (21) solving the hydrostatic part of the model and we focus on the correction step (22)-(23).

2.2.1. *Variational formulation.* The correction step (22)-(23) writes,

$$\begin{aligned} H^{n+1} &= H^{n+1/2}, && (24)\\ (H\mathbf{u})^{n+1} + \Delta t^n \nabla_{sw}\, p_{nh}^{n+1} &= (H\mathbf{u})^{n+1/2}, && (25)\\ \mathrm{div}_{sw}\,(\mathbf{u}^{n+1}) &= 0. && (26) \end{aligned}$$

For the sake of clarity, in the following we will drop the notation with a bar and we denote p instead of $\bar{p}_{nh}$. Likewise we drop the superscript $^{n+1}$ for the corrected states.

The system of equations (25)-(26) is a mixed problem in velocity/pressure, its approximation leads to a variational mixed problem. We introduce the spaces:

$$\begin{aligned} V &= \{\mathbf{v} = (v_1, v_2) \in (L^2(\Omega))^2 | \mathrm{div}_{sw}\,(\mathbf{v}) \in L^2(\Omega)\}, && (27)\\ Q &= \{q \in L^2(\Omega) | \nabla_{sw}\, q \in (L^2(\Omega))^2\}, && (28) \end{aligned}$$

and

$$\begin{aligned} V_0 &= \{\mathbf{v} \in V,\ v|_\Gamma = 0\}, && (29)\\ Q_0 &= \{q \in Q,\ q|_\Gamma = 0\}. && (30) \end{aligned}$$

The variational problem writes:

Find $\mathbf{u} \in V_0$, $p \in Q$ such that

$$\int_\Omega (H\mathbf{u} + \Delta t^n \nabla_{sw}\, p) \cdot \mathbf{v}\, dx = \int_\Omega (H\mathbf{u})^{n+1/2} \cdot \mathbf{v}\ dx, \quad \forall\, \mathbf{v} \in V_0, \tag{31}$$

$$\int_\Omega \mathrm{div}_{sw}\,(\mathbf{u}) q\, dx = 0, \quad \forall q \in Q. \tag{32}$$

In this part, in order to simplify the problem, the velocity is taken in V_0 (which is not physically relevant in general), to eliminate the boundary term that will appear when the duality relation (12) is used in (31).

Indeed, introducing the bilinear forms

$$a(\mathbf{u}, \mathbf{v}) = \int_\Omega H\mathbf{u} \cdot \mathbf{v}\, dx, \quad \forall\, \mathbf{u}, \mathbf{v} \in V_0,$$

$$b(\mathbf{v}, q) = -\int_\Omega \mathrm{div}_{sw}\,(\mathbf{v}) q\, dx, \quad \forall \mathbf{v} \in V_0, \forall\, q \in Q,$$

the problem (31)-(32) becomes:

Find $p \in Q$ and $\mathbf{u} \in V_0$ such that

$$\frac{1}{\Delta t^n} a(\mathbf{u}, \mathbf{v}) + b(\mathbf{v}, p) = \frac{1}{\Delta t^n} a(\mathbf{u}^{n+1/2}, \mathbf{v}), \quad \forall \mathbf{v} \in V_0, \tag{33}$$

$$b(\mathbf{u}, q) = 0, \quad \forall q \in Q. \tag{34}$$

The two spaces V_0 and Q have been chosen to consider the variational problem without the boundary term

$$\int_\Gamma Hp\, v_1\, n\, ds \tag{35}$$

with n the unit outward normal vector defined by (6).

As well, to have a Dirichlet condition on the pressure instead of the velocity, the following problem can be considered.

Find $\mathbf{u} \in V$ and $p \in Q_0$ such that

$$\frac{1}{\Delta t^n} a(\mathbf{u}, \mathbf{v}) + b(\mathbf{v}, p) = \frac{1}{\Delta t^n} a(\mathbf{u}^{n+1/2}, \mathbf{v}), \quad \forall \mathbf{v} \in V, \tag{36}$$

$$b(\mathbf{u}, q) = 0, \quad \forall q \in Q_0. \tag{37}$$

In section 2.3, we will introduce other functional spaces to take into consideration the boundary conditions of the correction step coupled with the hyperbolic part.

2.2.2. *The pressure equation.* In this part, we are interested in deriving an equation for the pressure. Instead of considering the problem in velocity/pressure under the coupled form "div-grad", we consider an elliptic problem leading to an uncoupled equation for the pressure. This is in analogy with the Poisson equation derived from the Euler equations by the projection scheme of Chorin-Temam [35, 17]. In order to obtain the pressure equation, we start from the problem (36)-(37) and take a specific value for $\mathbf{v}$.

Formally, let us take $\mathbf{v}$ of the form $\mathbf{v} = \frac{\nabla_{sw}\, q}{H}$ with $q \in Q_0$ defined by (30).

Then, we notice that

$$a\left(\mathbf{w}, \frac{\nabla_{sw}\, q}{H}\right) = b(\mathbf{w}, q) \quad \forall \mathbf{w} \in V, \ \ \forall q \in Q_0.$$

Indeed, with (12), we get

$$\begin{aligned} a(\mathbf{w},\mathbf{v}) &= a\left(\mathbf{w},\frac{\nabla_{sw}\,q}{H}\right)\\ &= \int_\Omega \mathbf{w}\cdot\nabla_{sw}\,q\,dx\\ &= -\int_\Omega \mathrm{div}_{sw}\,(\mathbf{w})q\,dx\\ &= b\,(\mathbf{w},q). \end{aligned}$$

So, using (34), we have

$$a\left(\mathbf{u},\frac{\nabla_{sw}\,q}{H}\right)=0\quad\forall q\in Q_0. \tag{38}$$

Then, (33) reduces to:

$$\left(\frac{\nabla_{sw}\,q}{H},\nabla_{sw}\,p\right) = \frac{1}{\Delta t^n}a\left(\mathbf{u}^{n+1/2},\frac{\nabla_{sw}\,q}{H}\right)\quad\forall q\in Q_0. \tag{39}$$

Let us introduce the shallow water version of the Laplacian operator Δ_{sw} defined by

$$\Delta_{sw}\,p=\mathrm{div}_{sw}\left(\frac{\nabla_{sw}\,p}{H}\right), \tag{40}$$

and the space

$$Q_{0,sw}=\{q\in Q_0|\mathrm{div}_{sw}\left(\frac{\nabla_{sw}\,q}{H}\right)\in L^2(\Omega)\}.$$

Using (12) and (40), we get

$$(\Delta_{sw}\,p,q) = \frac{1}{\Delta t^n}\left(\mathrm{div}_{sw}\,(\mathbf{u}^{n+1/2}),q\right),\quad\forall q\in Q_{0,sw}. \tag{41}$$

From (41), we deduce

$$\Delta_{sw}\,p = \frac{1}{\Delta t^n}\mathrm{div}_{sw}\,(\mathbf{u}^{n+1/2}), \tag{42}$$

$$p|_{\Gamma=0} = 0. \tag{43}$$

The resolution of the equations (42)-(43) allows to compute p and then to update the velocity at the correction step (25).

To obtain equation (42), which is independent of $\mathbf{u}$, it is equivalent to apply the operator div_{sw} to the equation (22) divided by H, and to use the shallow water free divergence condition (23) to eliminate $\mathbf{u}$.

Remark 2. The existence and uniqueness of the problems are not treated in this paper since it would require more developments. This subject will be explored in a forthcoming paper devoted to the two dimensional case. As well, one can ask about the inf-sup condition of the mixed problem (33)-(34), this property can be easily verified for the chosen spaces, indeed the Babuska-Brezzi [10, 34] condition has to be satisfied. Denoting by $\mathcal{B}$ the weak operator defined by $\forall\mathbf{v}\in V_0$, $\mathcal{B}\mathbf{v}=b(\mathbf{v},q),\forall q\in Q$, we have

$$\begin{aligned}\ker\mathcal{B}^t &= \{q\in Q|\mathcal{B}^tq=0\}\\ &= \{q\in Q|\int_\Omega\nabla_{sw}\,q\cdot\mathbf{v}\,dx=0\;\forall\mathbf{v}\in V_0\}.\end{aligned}$$

Choosing $\mathbf{v} \in (L^2(\Omega))^2$ and q such as $\nabla_{sw}\, q \in (L^2(\Omega))^2$, it follows that $\nabla_{sw}\, q = 0$, then, with(10), we get $q = 0$ and $\ker \mathcal{B}^t = 0$. Indeed, in contrast with Navier-Stokes equations for which the pressure is defined up to an additive constant, the pressure of the shallow water equations is fully defined. Therefore, the mixed problem (33)-(34) satisfies the inf-sup condition. A similar argument applies to the problem (36)-(37) to have the inf-sup condition.

2.3. **Boundary conditions.** In this section, we still consider that the hydrostatic part is provided and we study the compatibility of the boundary conditions between the hydrostatic part and the projection part. Therefore, the compatibility between the pressure and velocity at boundary needs to be studied. To this aim, we first provide the conditions required to impose a Dirichlet or a Neumann boundary condition for the pressure at the boundary on the variational formulation, and then, we couple these conditions with the hydrostatic part. Concerning the bathymetry, it is usual to impose a Neumann boundary condition for the bottom z_b at the hydrostatic level.

We consider a more general case taking the space V defined by (27) and we introduce the bilinear form

$$c(\mathbf{v}, p) = -\int_\Gamma Hp\, v_1\, n\, ds, \quad \forall \mathbf{v} \in V, p \in Q,$$

with n the unit outward normal vector defined by (6). In one dimension, $c(\mathbf{v}, p) = -(Hpv_1)|_{\Gamma_{out}} + (Hpv_1)|_{\Gamma_{in}}$.

Therefore instead of (33)-(34), we consider the problem:

Find $\mathbf{u} \in V$, $p \in Q$ such that,

$$\frac{1}{\Delta t^n} a(\mathbf{u}, \mathbf{v}) + b(\mathbf{v}, p) = \frac{1}{\Delta t^n} a(\mathbf{u}^{n+1/2}, \mathbf{v}) + c(\mathbf{v}, p), \quad \forall\, \mathbf{v} \in V, \tag{44}$$

$$b(\mathbf{u}, q) = 0, \quad \forall q \in Q. \tag{45}$$

Notice that $\mathrm{div}_{sw}\,(\mathbf{u}) = \nabla_0 \cdot (H\mathbf{u}) + \mathbf{u} \cdot (\mathbf{n_s} + \mathbf{n_b})$ and $\nabla_{sw}\, p = H\nabla_0(p) - p(\mathbf{n_s} + \mathbf{n_b})$ with ∇_0 defined by (7) and $\mathbf{n_s}$ (resp. $\mathbf{n_b}$) the (non-unit) normal vector at the surface (resp. at the bottom)

$$\mathbf{n_s} = \begin{pmatrix} -\frac{\partial \eta}{\partial x} \\ 1 \end{pmatrix}, \qquad \mathbf{n_b} = \begin{pmatrix} -\frac{\partial z_b}{\partial x} \\ 1 \end{pmatrix}.$$

With that notation, the relation (12) rewrites

$$\int_\Omega \mathrm{div}_{sw}\,(\mathbf{u})\, dx = \int_\Gamma Hu\, n\, ds + \int_\Omega \mathbf{u} \cdot (\mathbf{n_s} + \mathbf{n_b})\, dx.$$

Hence, to satisfy the divergence free condition, the velocity $\mathbf{u}$ should verify

$$\int_\Gamma Hu\, n\, ds = -\int_\Omega \mathbf{u} \cdot (\mathbf{n_s} + \mathbf{n_b})\, dx.$$

Dirichlet boundary condition for the pressure. From the variational formulation of the projection scheme, due to the term (35), a natural boundary condition for the pressure is a Dirichlet condition, in the sense that the pressure at the boundary Γ_i, $i = in$ or $i = out$, appears in the boundary term of the variational form $\int_{\Gamma_i} Hpv_1 n\, ds$. At $\Gamma_i, (i = in, out)$, if $p|_{\Gamma_i} = p_0$ then $c(\mathbf{v}, p) = \int_{\Gamma_i} Hp_0 v_1 n\, ds$ and we take $\mathbf{v} \in V$, $q \in Q_i$ with

$$Q_i = \{q \in L^2(\Omega) | \nabla_{sw}\, q \in (L^2(\Omega))^2, q|_{\Gamma_i} = 0\}.$$

In the case $p|_\Gamma = p_0$, the problem writes:

Find $\mathbf{u} \in V, p - p_0 \in Q_0 = \{q \in Q, \quad q|_\Gamma = 0\}$, such that

$$\begin{aligned}\frac{1}{\Delta t^n}\int_\Omega \left(H\mathbf{u}\cdot\mathbf{v} - p\,\mathrm{div}_{sw}(\mathbf{v})\right)\,dx &= \frac{1}{\Delta t^n}\int_\Omega H\mathbf{u}^{n+1/2}\cdot\mathbf{v}\,dx \\ &\quad -\int_\Gamma Hp_0v_1n\,ds \quad ,\forall \mathbf{v}\in V,\\ \int_\Omega q\,\mathrm{div}_{sw}(\mathbf{u})dx &= 0, \quad \forall q\in Q.\end{aligned}$$

Neumann boundary condition for the pressure. The Neumann boundary condition for the projection scheme is not natural and to enforce such a condition, the elliptic problem (39)-(41) has to be considered. Using this formulation, the velocity at the boundary is a part of the right hand side. Taking now $q \in Q_{sw}$, with $Q_{sw} = \{q \in Q|\mathrm{div}_{sw}(\frac{\nabla_{sw}p}{H}) \in L^2(\Omega)\}$, the problem is rewritten

$$\begin{aligned}\frac{1}{\Delta t^n}a(\mathbf{u},\mathbf{v}) + (\mathbf{v},\nabla_{sw}p) &= \frac{1}{\Delta t^n}a(\mathbf{u}^{n+1/2},\mathbf{v}) \quad \forall \mathbf{v}\in V,\\ (\Delta_{sw}p,q) + \frac{1}{\Delta t^n}\tilde{c}(p,q) &= \frac{1}{\Delta t^n}\left(\mathrm{div}_{sw}(\mathbf{u}^{n+1/2}),q\right) + \frac{1}{\Delta t^n}\int_\Gamma Huqnds\\ &\quad -\frac{1}{\Delta t^n}\int_\Gamma Hu^{n+1/2}qnds, \quad \forall q\in Q_{sw},\end{aligned}$$

with $\tilde{c}$, the bilinear form

$$\tilde{c}(p,q) = -\int_\Gamma (\Delta t^n \nabla_{sw}p|_1)\,q\,n\,ds. \tag{46}$$

Many studies have been done to choose an appropriate variational formulation for this problem. In [26] J-L. Guermond explores the different variational formulations in order to enforce a Neumann pressure boundary condition, in [28] some equivalent formulations are given to switch between Neumann and Dirichlet boundary conditions. As for the hyperbolic part, we still consider that we have imposed a Neumann boundary condition for the topography $\frac{\partial z_b}{\partial x}|_{\Gamma_i} = 0$, $\forall i = in, out$. Taking the normal component at the boundary Γ_i of the momentum equation at the second step of the splitting (25), it follows that

$$H\frac{\partial p}{\partial n}|_{\Gamma_i} + p|_{\Gamma_i}(\frac{\partial H}{\partial n}|_{\Gamma_i}) = \frac{H}{\Delta t^n}(u|_{\Gamma_i}^{n+1/2} - u|_{\Gamma_i}),$$

where the left hand side corresponds to the boundary terms (46) of the elliptic problem.

We denote $\frac{\partial H}{\partial n}|_{\Gamma_i} = \beta_i$, $i = in, out$.

- In case $\beta_i = 0$, a Neumann boundary condition for the pressure is deduced from a Dirichlet condition for u.

$$\frac{\partial p}{\partial n}|_{\Gamma_i} = \frac{1}{\Delta t^n}(u|_{\Gamma_i}^{n+1/2} - u|_{\Gamma_i}). \tag{47}$$

- In the other cases, it gives a mixed boundary condition

$$\frac{\partial p}{\partial n}|_{\Gamma_i} + \beta_i p|_{\Gamma_i} = \frac{1}{\Delta t^n}(u|_{\Gamma_i}^{n+1/2} - u|_{\Gamma_i}). \tag{48}$$

Then, in the two cases, we have imposed a Dirichlet velocity condition, that leads to take $\mathbf{v} \in V_i$ and $q \in Q$, with $i = in$ for the inflow or $i = out$ for the outflow where

$$V_i = \{\mathbf{v} = (v_1, v_2) \in (L^2(\Omega))^2 | \mathrm{div}_{sw}(\mathbf{v}) \in L^2(\Omega), v_{1|\Gamma_i} = 0\}. \tag{49}$$

Let us now give the coupling boundary conditions between the prediction step and the correction step. Indeed, in the projection part, boundary conditions need to be set in order to be consistent with the hydrostatic part.

Concerning the prediction step, we consider the well known Saint-Venant system and we assume that the Riemann invariant remains constant along the associated characteristic. This approach has been introduced in [11] and distinguishes fluvial and torrential boundaries depending on the Froude number $Fr = \frac{|u|}{c}$. Usual boundary conditions consist in imposing a flux $\mathbf{q}_0$ at the inflow boundary and a water depth at the outflow boundary. It is also classical to let a free outflow boundary, setting a Neumann boundary condition for the water depth and for the velocity. For both cases, we now give the boundary conditions that have to be set in the correction step.

We consider the first situation in which we set a flux at the inflow Γ_{in} and a given depth at the outflow Γ_{out}. Assuming a fluvial flow, this case consists in solving a Riemann problem at the interface Γ_{in} where the global flux is given by $\mathbf{q}_0 = (q_{01}, q_{02})^t = (Hu^{n+1/2}, Hw^{n+1/2})^t$. That gives the boundary values $H_0 = H_0^{n+1/2}$, $u_0 = \frac{q_{02}}{H_0^{n+1/2}}$ and $w_0 = \frac{q_{02}}{H_0^{n+1/2}}$ from the hyperbolic part. This leads to obtain a Dirichlet condition for the pressure at the left boundary of the correction part.

Moreover, if H is given for the outflow, we preconize to give a mixed condition for the pressure that corresponds to the boundary condition (48)

$$\begin{aligned} p|_{\Gamma_{in}} &= 0, \\ \left.\frac{\partial p}{\partial n}\right|_{\Gamma_{out}} + p\left.\frac{\partial H}{\partial n}\right|_{\Gamma_{out}} &= 0, \end{aligned}$$

that leads to take $\mathbf{u} \in V_{out}$, with the definition (49) and

$$p \in Q_{in} = \{q \in L^2(\Omega) | \nabla_{sw}\, q \in L^2(\Omega), \quad q_{|\Gamma_{in}} = 0\}.$$

We now consider the second situation in which we still impose a flux $\mathbf{q}_0$ at the inflow and we set a free outflow boundary. In this case, we assume the two Riemann invariants are constant along the outgoing characteristics of the hyperbolic part (see [11]), therefore, we have a Neumann boundary condition for $H^{n+1/2}$ and $u^{n+1/2}$.

$$\left.\frac{\partial H}{\partial n}\right|_{\Gamma_{out}} = 0, \qquad \left.\frac{\partial \mathbf{u}^{n+1/2}}{\partial n}\right|_{\Gamma_{out}} = 0.$$

Preserving these conditions at the correction step, it gives a Neumann boundary condition for the pressure of type (47)

$$\left.\frac{\partial p}{\partial n}\right|_{\Gamma_{out}} = 0.$$

For an inflow given, the functional spaces will be defined by

$$\mathbf{u} \in V_{out},\ p \in Q_{in}.$$

3. Numerical approximation.

3.1. **Discretization.** This section is devoted to the numerical approximation and gives mainly details about the correction step. Let us be given a subdivision of Ω with N vertices $x_1 < x_2 < ... < x_N$ and we define the space step $\Delta x_{i+1/2} = x_{i+1} - x_i$. We also note $\Delta x_i = x_{i+1/2} - x_{i-1/2}$ with $x_{i+1/2} = \frac{x_i + x_{i+1}}{2}$.

Prediction part. For the prediction step (21) i.e the hydrostatic part of the model, we use a finite volume scheme. We introduce the finite volume cells C_i centered at vertices x_i such that $\Omega = \cup_{i=1,N} C_i$. Then, the approximate solution X_i^n at time t^n

$$X_i^n \approx \frac{1}{\Delta x_i} \int_{C_i} X(x, t^n) dx,$$

is solution of the numerical scheme

$$X_i^{n+1} = X_i^n - \sigma_i^n \left(\mathcal{F}_{i+1/2}^n - \mathcal{F}_{i-1/2}^n \right) + \sigma_i^n \mathcal{S}_i^n,$$

where $\sigma_i^n = \frac{\Delta t^n}{\Delta x_i}$ and $\mathcal{F}$ (resp. $\mathcal{S}$) is a robust and efficient discretization of the conservative flux $F(X)$ (resp. the source term $S(X)$). The time step is determined through a classical CFL condition. Many numerical fluxes and discretizations are available in the literature [9, 23, 31], we choose a kinetic based solver [5] coupled with the hydrostatic reconstruction technique [4].

Correction part. Concerning the correction step (22)-(23), we consider the discrete problem corresponding to the mixed problem (33)-(34). We approach $(V_0,\ Q)$ by the finite dimensional spaces $(V_{0h},\ Q_h)$ and we note

$$N = \dim(V_{0h}), \qquad M = \dim(Q_h).$$

We also denote by $(\varphi_i)_{i=1,N}$ and $(\phi_l)_{l=1,M}$ the basis functions of V_{0h} and Q_h respectively. The finite dimensional spaces will be specified later on. We approximate $(\mathbf{u}, p) \in (V_0, Q)$ by $(\mathbf{u}_h, p_h) \in (V_{0h}, Q_h)$ such that

$$\mathbf{u}_h(x) = \sum_{i=1}^{N} \begin{pmatrix} u_i \\ w_i \end{pmatrix} \varphi_i(x), \qquad p_h(x) = \sum_{l=1}^{M} p_l\, \phi_l(x).$$

Therefore, we consider the discrete problem corresponding to (33)-(34).
Find $\mathbf{u}_h \in V_{0h}$, $p_h \in Q_h$ such that

$$\frac{1}{\Delta t^n} a(\mathbf{u}_h, \mathbf{v}_h) + b(\mathbf{v}_h, p_h) = \frac{1}{\Delta t^n} a(\mathbf{u}_h^{n+1/2}, \mathbf{v}_h), \quad \forall \mathbf{v}_h \in V_{0h}, \tag{50}$$

$$b(\mathbf{u}_h, q_h) = 0, \quad \forall q_h \in Q_h. \tag{51}$$

Let us introduce the mass matrix M_H given by

$$M_H = \left(\int_\Omega H \varphi_i \varphi_j dx \right)_{1 \le i,j \le N},$$

and the two matrices B^t, B defined by

$$B^t = \left(\int_\Omega \nabla_{sw}(\phi_l) \varphi_i dx \right)_{1 \le l \le M, 1 \le i \le N}, B = -\left(\int_\Omega \mathrm{div}_{sw}(\varphi_j) \phi_l dx \right)_{1 \le l \le M, 1 \le j \le N},$$

and we denote

$$U = \begin{pmatrix} u_1 \\ \vdots \\ u_N \\ w_1 \\ \vdots \\ w_N \end{pmatrix}, \qquad P = \begin{pmatrix} p_1 \\ \vdots \\ p_M \end{pmatrix},$$

Therefore, the problem (50)-(51) becomes

$$\begin{pmatrix} \frac{1}{\Delta t^n} A_H & B^t \\ B & 0 \end{pmatrix} \begin{pmatrix} U \\ P \end{pmatrix} = \begin{pmatrix} \frac{1}{\Delta t^n} A_H U^{n+1/2} \\ 0 \end{pmatrix},$$

with

$$A_H = \begin{pmatrix} M_H & 0 \\ 0 & M_H \end{pmatrix}.$$

Assuming that M_H is invertible and eliminating the velocity U, we obtain the following equation

$$B A_H^{-1} B^t P = \frac{1}{\Delta t^n} B U^{n+1/2}, \tag{52}$$

that is a discretization of the elliptic equation (42) of Sturm-Liouville type governing the pressure p.

We now take into account the boundary conditions in the more general problem (44)-(45). The velocity $\mathbf{u}$ is approximated by $\mathbf{u}_h \in V_h$, and the discrete problem is then written:

Find $(\mathbf{u}_h, p_h) \in (V_h, Q_h)$ such that

$$\begin{aligned} \frac{1}{\Delta t^n} a(\mathbf{u}_h, \mathbf{v}_h) + b(\mathbf{v}_h, p_h) &= \frac{1}{\Delta t^n} a(\mathbf{u}_h^{n+1/2}, \mathbf{v}_h) + \frac{1}{\Delta t^n} c(\mathbf{u}_h, p_h), \quad \forall \mathbf{v}_h \in V_h, \\ b(\mathbf{u}_h, q_h) &= 0 \quad \forall q_h \in Q_h. \end{aligned}$$

Considering the matrix $\Delta t^n C = (c(\varphi_i, \phi_l))_{1 \le l \le M, 1 \le i \le N}$ that contains the boundary terms, the equation (52) becomes

$$B A_H^{-1} (B^t - C) P = \frac{1}{\Delta t^n} B U^{n+1/2}.$$

This approach is suitable for the finite element approximation that is given in the next section. However, it implies to invert a mass matrix M_H that is not diagonal and depends on the water depth H. In practice, we use the mass lumping technique introduced by Gresho ([25]) to avoid inverting the mass matrix in projection methods for Navier-Stokes incompressible system.

3.2. **Finite element $\mathbb{P}_1/\mathbb{P}_0$.** It has been seen in [1] that the discrete entropy is satisfied if we use a finite difference scheme on a staggered grid, then we choose the specific pair $\mathbb{P}_1/\mathbb{P}_0$ in order to satisfy the entropy properties.

The problem is solved by the mixed finite element approximation $\mathbb{P}_1/\mathbb{P}_0$ (see [34]) on the domain $\Omega = \cup_{l=1}^{M} K_l$ ($M = N-1$ with N the number of nodes), where the velocity is approximated by a continuous linear function and the pressure is approximated by a discontinuous piecewise constant function over each element

$$\mathbf{u}_h \in V_h = \{\mathbf{v}_h \in (\mathcal{C}^0(\Omega))^2 \mid \ \mathbf{v}_h|_{K_l} \in \mathbb{P}_1^2, \forall l = 1, \dots, N-1\},$$

and

$$p_h \in Q_h = \{q_h \mid \ q_h|_{K_l} \in \mathbb{P}_0 \ , \ \forall l = 1, \dots, M-1\}.$$

Using the discretization given in 3.1, we denote by $K_{i+1/2}$ the finite element cell $[x_i, x_{i+1}]$, then the pressure is constant on the finite element $K_{i+1/2}$.

For the sake of clarity, in this situation, let $\left(\phi_{j+1/2}\right)_{1 \le j \le M}$ be the basis functions for the pressure p_h, and $(\varphi_i)_{1 \le i \le N}$ the basis functions for the velocity $\mathbf{u}_h$, and set

$$\mathbf{u}_h(x) = \sum_{i=1}^{N} \begin{pmatrix} u_i \\ w_i \end{pmatrix} \varphi_i(x), \quad p_h(x) = \sum_{j=1}^{M} p_{j+1/2}\, \phi_{j+1/2}(x).$$

We note $\zeta = H + 2z_b$ and assume ζ is approximated by a piecewise linear function ζ_h, namely $\zeta_h(x) = \sum_{i=i}^{N} \zeta_i \varphi_i(x)$. We also note $\frac{\partial \zeta_h}{\partial x}|_{i+1/2} = \frac{\zeta_{i+1}-\zeta_i}{\Delta x_{i+1/2}} = \frac{\chi_{i+1/2}}{\Delta x_{i+1/2}}$ the constant gradient of ζ_h on the element $K_{i+1/2}$.

Remark 3. In the context of the discontinuous Galerkin method, using $\partial_x \phi_{j+1/2}(x) = \delta_j(x) - \delta_{j+1}(x)$ in the sense of distribution, it gives a distributional derivative for the pressure $\partial_x p_h(x) = \sum_j \left(p_{j+1/2} - p_{j-1/2}\right) \delta_j(x)$.

We denote $\underline{\varphi} = (\varphi, \varphi)^t$, then the shallow water gradient operator is written

$$\int_\Omega \nabla_{sw}(p_h) \cdot \underline{\varphi_i}\, dx = \begin{pmatrix} H_i(p_{i+1/2} - p_{i-1/2}) + \frac{p_{i-1/2}}{2}\chi_{i-1/2} + \frac{p_{i+1/2}}{2}\chi_{i+1/2} \\ -(\Delta x_{i+1/2} p_{i+1/2} + \Delta x_{i-1/2} p_{i-1/2}) \end{pmatrix}.$$

Similarly, after integrating by part, the shallow water divergence operator writes

$$\begin{aligned} \int_\Omega \mathrm{div}_{sw}\left(\mathbf{u}_h\right) \phi_{j+1/2}\, dx &= H_{j+1}u_{j+1} - H_j u_j - \frac{u_j + u_{j+1}}{2}\left(\zeta_{j+1} - \zeta_j\right) \\ &\quad + \Delta x_{j+1/2}(w_j + w_{j+1}). \end{aligned}$$

In one dimension, this approach corresponds to a staggered-grid finite-difference method where the velocity is computed at the nodes and the pressure is computed at the middle nodes. The discretization we obtain corresponds exactly to the finite difference scheme given in [1], and then, the properties established in [1] are conserved.

3.3. **Finite element $\mathbb{P}_1$-iso-$\mathbb{P}_2/\mathbb{P}_1$.** In this part, we propose to give an approximation $\mathbb{P}_1$-iso-$\mathbb{P}_2$ for the velocity and $\mathbb{P}_1$ for the pressure. This pair has been chosen in order to prepare the two dimensional method for which the Inf-Sup condition is verified with this couple (see [34]). Moreover, to satisfy the discrete entropy, as explained in [1], it is necessary to have a staggered grid. We give here an analogy for the one dimensional problem.

For the one dimensional $\mathbb{P}_1$-iso-$\mathbb{P}_2/\mathbb{P}_1$, we consider two meshes $\mathcal{K}_h$ (the same as before) and $\mathcal{K}_{2h}$ with $K_{h,i+1/2} = [x_i, x_{i+1}]$ and $K_{2h,j} = [x_{2j-1}, x_{2j+1}]$ the finite elements defined on the respective meshes $\mathcal{K}_h$ and $\mathcal{K}_{2h}$ such that $\mathcal{K}_h = \cup_{i=1}^{N-1} K_{h,i+1/2}$ and $\mathcal{K}_{2h} = \cup_{j=1}^{M-1} K_{2h,j}$ with N the total number of vertices of $\mathcal{K}_h$ and $M = (N-1)/2$ (assuming N odd), the number of vertices of $\mathcal{K}_{2h}$. Therefore, the approximation spaces V_h and Q_h are defined by

$$\begin{aligned} V_h &= \left\{ \mathbf{v}_h \in C^0(\Omega)^2 |\ \mathbf{v}_h|_{K_h,i} \in \mathbb{P}_1^2, \forall i = 1, \cdots, N-1 \right\}, \\ Q_h &= \left\{ q_h \in C^0(\Omega) |\ q_h|_{K_{2h,j}} \in \mathbb{P}_1, \forall j = 1, ..., M-1 \right\}. \end{aligned}$$

Then, the velocity and the pressure are written

$$p_h(x) = \sum_{j=1}^{M} p_j \phi_j, \quad \mathbf{u}_h(x) = \sum_{i=1}^{N} \begin{pmatrix} u_i \\ w_i \end{pmatrix} \varphi_i. \tag{53}$$

where $(\phi_j)_{1\le j\le M}$ are the basis functions for the pressure p_h, and $(\varphi_i)_{1\le i\le N}$ the basis functions for the velocity $\mathbf{u}_h$.

In figure 2, the dashed lines are the usual elementary basis functions of $\mathbb{P}_1$ on the mesh $\mathcal{K}_h$, while the continuous lines are the basis functions on the mesh $\mathcal{K}_{2h}$. The divergence operator, for all $j = 1, M$, writes

$$\int_\Omega \mathrm{div}_{sw}(\mathbf{u}_h)\phi_j\, dx = \sum_{K_h \in \mathcal{K}_h} \int_{K_h} \mathrm{div}_{sw}(\mathbf{u}_h)\phi_j\, dx.$$

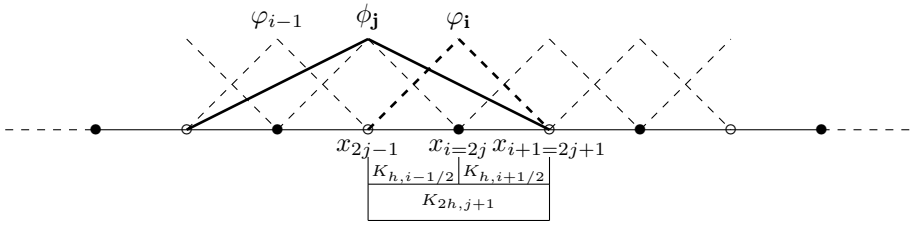

FIGURE 2. Representation of the basis functions.

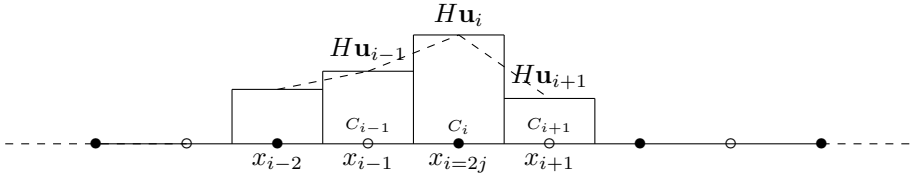

FIGURE 3. Representation of the discretization of the function $(H\mathbf{u})$ and representation of the finite volume cell $C_i = [x_{i-1/2}, x_{i+1/2}]$.

We use a linear interpolation for $H\varphi_j$ in the computation of $\int_{K_{h,i+1/2}} H\varphi_i\, dx$, and we consider that $\Delta x_i = \Delta x \quad \forall i = 1, \ldots, N$ for the sake of simplicity. We still approximate ζ by ζ_h defined before.

The discrete shallow water divergence operator is computed for all nodes x_j of the mesh $\mathcal{K}_{2h}$ and therefore, denoting $i = 2j-1$, it can be written, $\forall j = 1, M$

$$\begin{aligned}
\int_\Omega \mathrm{div}_{sw}(\mathbf{u}_h)\phi_j\, dx \;=\; & \left(\frac{1}{4}H_{i+2}u_{i+2} + \frac{H_{i+1}}{2}u_{i+1}\right) - \left(\frac{1}{4}H_{i-2}u_{i-2} + \frac{H_{i-1}}{2}u_{i-1}\right) \\
& - \left(\chi_{i-1/2}m_{i,j}^{i-1/2} + \chi_{i+1/2}m_{i,j}^{i+1/2}\right)u_i \\
& - \left(\chi_{i-3/2}m_{i-2,j}^{i-3/2}\right)u_{i-2} - \left(\chi_{i+3/2}m_{i+2,j}^{i+3/2}\right)u_{i+2} \\
& - \left(\chi_{i-1/2}m_{i-1,j}^{i-1/2} + \chi_{i-3/2}m_{i-1,j}^{i-3/2}\right)u_{i-1} \\
& - \left(\chi_{i+1/2}m_{i+1,j}^{i+1/2} + \chi_{i+3/2}m_{i+1,j}^{i+3/2}\right)u_{i+1} \\
& + (2m_{i,j}^{i+1/2})w_i \\
& + \left(m_{i-1,j}^{i-1/2} + m_{i-1,j}^{i-3/2}\right)w_{i-1} + \left(m_{i+1,j}^{i+1/2} + m_{i+1,j}^{i+3/2}\right)w_{i+1} \\
& + (m_{i-2,j}^{i-3/2})w_{i-2} + m_{i+2,j}^{i+3/2}w_{i+2},
\end{aligned}$$

with $m_{i,j}^{i+1/2} = \int_{K_{h,i+1/2}} \varphi_i\phi_j dx$.

Similarly, the shallow water gradient operator is obtained for all the nodes x_i of the mesh $\mathcal{K}_h$. However, we distinguish the gradient at the nodes of the elements K_{2h} from the ones at the interior. In other words, for all the nodes x_i of the mesh $\mathcal{K}_{2h}$, the gradient operator is defined by

$$\int_\Omega \nabla_{sw}\, p_h \cdot \underline{\varphi}_{(i=2j-1)}\, dx\Big|_1 \;=\; \frac{H_i}{4}\,(p_{j+1} - p_{j-1})$$

$$
\begin{aligned}
&+\chi_{i-1/2}\left(m_{i,j}^{i-1/2}p_j + m_{i,j-1}^{i-1/2}p_{j-1}\right)\\
&+\chi_{j+1/2}\left(m_{i,j}^{i+1/2}p_j + m_{i,j+1}^{i+1/2}p_{j+1}\right),\\
\int_\Omega \nabla_{sw}\, p_h \cdot \underline{\varphi}_{(i=2j-1)}\, dx\Big|_2 &= -2m_{i,j}^{i+1/2}p_j - m_{i,j}^{i-1/2}p_{j-1} - m_{i,j}^{i+1/2}p_{j+1}.
\end{aligned}
$$

On the other hand, for all the nodes x_i such that i is even

$$
\begin{aligned}
\int_\Omega \nabla_{sw}\, p_h \cdot \underline{\varphi}_{(i=2j)}\, dx\Big|_1 &= \frac{H_i}{2}\left(p_{j+1} - p_j\right)\\
&+\left(\chi_{i-1/2}m_{i,j}^{i-1/2} + \chi_{i+1/2}m_{i,j}^{i+1/2}\right)p_j\\
&+\left(\chi_{i-1/2}m_{i,j+1}^{i-1/2} + \chi_{i+1/2}m_{i,j+1}^{i+1/2}\right)p_{j+1},\\
\int_\Omega \nabla_{sw}\, p_h \cdot \underline{\varphi}_{(i=2j)}\, dx\Big|_2 &= -\left(m_{i,j}^{i-1/2} + m_{i,j}^{i+1/2}\right)p_j - \left(m_{i,j+1}^{i-1/2} + m_{i,j+1}^{i+1/2}\right)p_{j+1}.
\end{aligned}
$$

With the discretization of the shallow water operators given above, we are able to validate the scheme for the first order method and the second order method.

3.4. **Towards a second order approximation.** In this section, we give some modifications of the previous scheme to improve the accuracy.

3.4.1. *Second order approximation in space.* A formally second order scheme in space has been developed for the hydrostatic shallow water system in [4], using a limited reconstruction of the variables. We use this reconstruction in the finite volume scheme applied to the hyperbolic part. For the correction part, we use the scheme presented in the previous section but a higher order accuracy could be used like a $\mathbb{P}_2 - \mathbb{P}1$ approximation for instance.

3.4.2. *Second order approximation in time.* For hyperbolic conservation laws, the second-order accuracy in time is usually recovered by the Heun method [8, 9] which is a slight modification of the second order Runge-Kutta method. The second order scheme presented here is an adaptation of the Heun scheme which takes into account the CFL constraint for each time step. More precisely, for a system written under the simplified form

$$\frac{\partial y}{\partial t} = f(y), \tag{54}$$

the scheme writes

$$
\begin{aligned}
\tilde{y}^{n+1} &= y^n + \Delta t_1^n f(y^n), &(55)\\
\tilde{y}^{n+2} &= \tilde{y}^{n+1} + \Delta t_2^n f(\tilde{y}^{n+1}), &(56)\\
y^{n+1} &= \alpha y^n + \beta \tilde{y}^{n+2}, &(57)
\end{aligned}
$$

where Δt_1^n and Δt_2^n respectively satisfy the CFL conditions associated with y^n and $\tilde{y}^{n+1}$. Using a Taylor expansion, it can be verified that this is a second order scheme in time if the following relations hold

$$
\begin{aligned}
\Delta t^n &= \frac{2\Delta t_1^n \Delta t_2^n}{\Delta t_1^n + \Delta t_2^n}, &(58)\\
\beta &= \frac{(\Delta t^n)^2}{2\Delta t_1^n \Delta t_2^n}, &(59)\\
\alpha &= 1 - \beta. &(60)
\end{aligned}
$$

Since, $\alpha, \beta \geq 0$, $\tilde{y}^{n+1}$ is a convex combination of y^n and $\tilde{y}^{n+2}$ so the scheme preserves the positivity.

By analogy, the idea is to apply this method to the prediction-correction scheme. To this aim, we rewrite the system (17)-(18) under the form

$$\begin{aligned} \frac{\partial X}{\partial t} &= f(X) - R_{nh}, && (61)\\ \mathrm{div}_{sw}\left(\tilde{\mathbf{u}}\right) &= 0 && (62) \end{aligned}$$

where R_{nh} is defined by (20) and $f(x) = -\frac{\partial F(X)}{\partial x} + S(X)$ with F and S defined by (19) and (20). We replace each step (55)-(56) by the prediction-correction step (21)-(22)

$$\begin{aligned} \tilde{X}^{n+1-} &= X^n + \Delta t_1^n f(X^n), && (63)\\ \tilde{X}^{n+1} &= \tilde{X}^{n+1-} - \Delta t_1^n \tilde{R}_n^{n+1}, && (64)\\ \mathrm{div}_{sw}\left(\tilde{\mathbf{u}}^{n+1}\right) &= 0, && (65) \end{aligned}$$

$$\begin{aligned} \tilde{X}^{n+2-} &= \tilde{X}^{n+1} + \Delta t_2^n f(\tilde{X}^{n+1}), && (66)\\ \tilde{X}^{n+2} &= \tilde{X}^{n+2-} - \Delta t_2^n \tilde{R}_{nh}^{n+2}, && (67)\\ \mathrm{div}_{sw}\left(\tilde{\mathbf{u}}^{n+2}\right) &= 0, && (68) \end{aligned}$$

and then (57) becomes

$$X^{n+1} = \alpha X^n + \beta \tilde{X}^{n+2}. \quad (69)$$

Notice that the divergence free condition is not satisfied by X^{n+1} but it is satisfied for each intermediate steps (64) and (67).

With these modifications, we improve the accuracy of the global scheme, some parts of which are formally "second order". But the proof of the convergence orders is a difficult problem that we do not address here. These difficulties have been encountered and have been studied for the Navier-Stokes problem by J-L.Guermond and J.Shen in [27] (see also [21, 22]).

The convergence order has been computed for the elevation and the pressure in the figures 6, 7 and 8 (see section 4.1).

4. **Analytical solutions.**

4.1. **Validation with an analytical solution.**

In [1],[13] some analytical solutions of the model (2)-(5) have been presented and they allow to validate the numerical method. We consider the propagation of a solitary wave on a flat bottom ($z_b = cte$). This solution has the form

$$\begin{aligned} H &= H_0 + a\left(\mathrm{sech}\left(\frac{x - c_0 t}{l}\right)\right)^2, && (70)\\ u &= c_0\left(1 - \frac{d}{H}\right), && (71)\\ w &= -\frac{a c_0 d}{lH}\mathrm{sech}\left(\frac{x - c_0 t}{l}\right)\mathrm{sech}'\left(\frac{x - c_0 t}{l}\right), && (72)\\ p &= \frac{a c_0^2 d^2}{2 l^2 H^2}\left((2H_0 - H)\left(\mathrm{sech}'\left(\frac{x - c_0 t}{l}\right)\right)^2\right., \end{aligned}$$

$$+ H\text{sech}\left(\frac{x-c_0t}{l}\right)\text{sech}''\left(\frac{x-c_0t}{l}\right)\Big), \tag{73}$$

with $d, a, H_0 \in \mathbb{R}$, $H_0 > 0$, $a > 0$ and

$$c_0 = \frac{l}{d}\sqrt{\frac{gH_0^3}{l^2 - H_0^2}}, \quad l = \sqrt{\frac{H_0^3}{a} + H_0^2} \tag{74}$$

The solitary wave is a particular case where dispersive contributions are counterbalanced by non linear effects so that the shape of the wave remains unchanged during the propagation. The propagation of the solitary wave has been simulated for the parameters $a = 0.4\,m, H_0 = 1\,m$, and $d = 1\,m$ over a domain of $45\,m$ with 9000 nodes. At time $t = 0$, the solitary wave is positioned inside the domain. The results presented in figure 4 show the different fields, namely the elevation, the components of velocity and the total pressure at different times, and the comparison with the analytical solution at the last time.

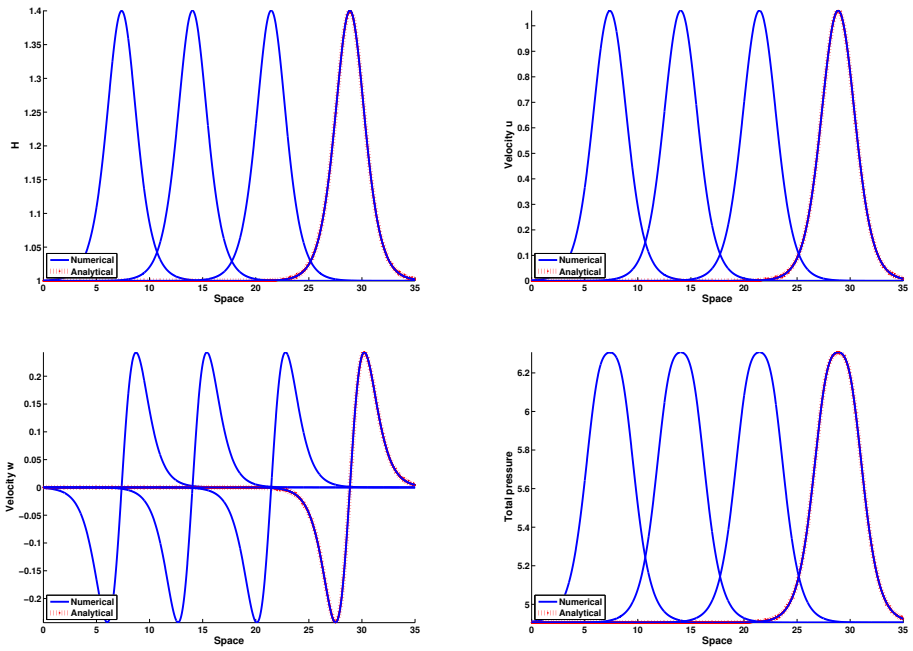

FIGURE 4. Propagation of the solitary wave at times $1.00008\,s, 1.9009\,s, 3.9017\,s$ and $5.9025\,s$. Comparison with analytical solution at time $t = 5.9025\,s$.

In the projection step, the greatest difficulty is to compute the pressure corresponding to the boundary conditions of the hyperbolic part (as seen in 2.3). The solution near the boundary has been confronted to the analytical solution. In the following result, we set a Neumann boundary condition on the non hydrostatic pressure with the parameters given below. As shown in the figure 4.1, the pressure is well estimated at the outflow boundary and allows the wave to leave the domain with a good behavior. The inflow boundary condition has been tested with this

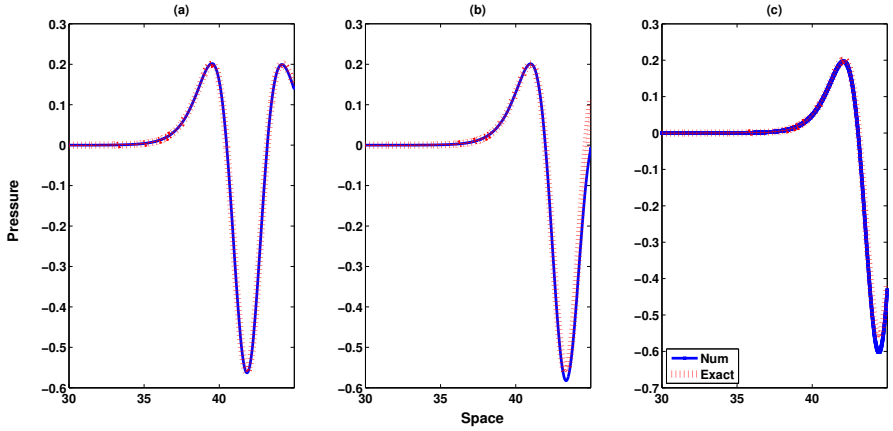

FIGURE 5. Non hydrostatic pressure profile at right boundary ($x = 45\,m$) (a): $t = 9.4044\,s$ (b): $t = 9.8046\,s$ (c): $t = 10.1048\,s$.

same test case and gives similar results. We are able to let the solitary wave enter in the domain with a good approximation of the elevation.

The numerical simulations for the first and the second order method are compared with the analytical solution and the L^2- error has been evaluated over different meshes of sizes from 395 nodes to 1695 nodes (see figures 6, 7, 8).

With the parameters given above, for the first order method it gives a convergence rate for H close to 1 for the two computations, i.e $\mathbb{P}_1/\mathbb{P}_0$ and $\mathbb{P}_1$-iso-$\mathbb{P}_2/\mathbb{P}_1$. For the second order scheme, it gives a convergence order close to two (see Fig.6). Same results have been also obtained for the velocity (see Fig.7).

In figure 8, the convergence rate has been computed for the pressure and we can observe that, for the first order method, the convergence rate of the pressure error is close to the first order, while the second order scheme gives a first order convergence rate for the pressure error.

Notice that the parameters set to validate the method lead to have a significant non hydrostatic pressure (see the figure 4.1) and then, the results show the ability of the method to preserve the solitary wave over the time.

The numerical results have also been obtained for the Thacker's test presented in [1], with the same convergence rate as the $\mathbb{P}_1/\mathbb{P}_0$ method.

4.2. **Partial comparison with the Green-Naghdi model.** In this part, we propose to compare the two models using an analytical solution of the Green-Naghdi model. As mentioned in Remark 1, the solution method presented in this paper does not apply immediately to the Green-Naghdi model. So, we just propose here a comparison with an analytical solution of the Green-Naghdi equations. In [13], it has been adduced that the analytical solitary wave of the Green-Naghdi model can be written in the same form as (70)-(73) with the parameters:

$$c_0 = \frac{2}{\sqrt{3}}\frac{l}{d}\sqrt{\frac{gH_0^3}{l^2 - H_0^2}}, \quad l = \frac{2}{\sqrt{3}}\sqrt{\frac{H_0^3}{a} + H_0^2}. \tag{75}$$

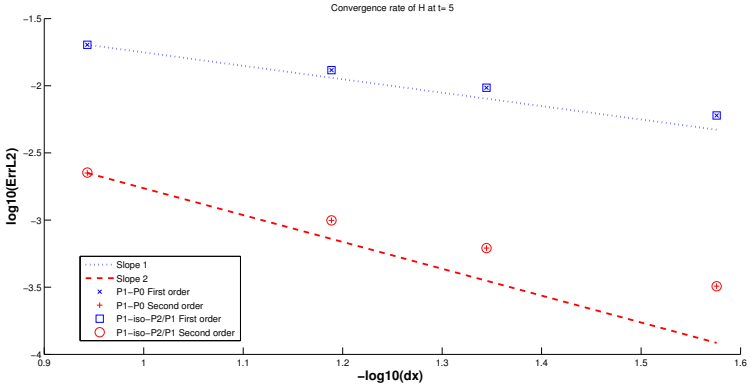

FIGURE 6. Convergence rate - Computation of the L_2-error of the solution H at time $t = 5s$ for the first and the second order scheme and comparison for $\mathbb{P}_1/\mathbb{P}_0$ and $\mathbb{P}_1$-iso-$\mathbb{P}_2/\mathbb{P}_1$ scheme.

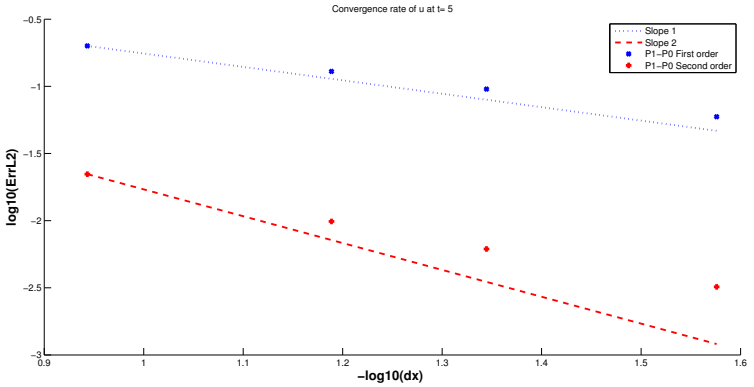

FIGURE 7. Convergence rate - Computation of the L_2-error of the solution u at time $t = 5s$ for the first and the second order scheme.

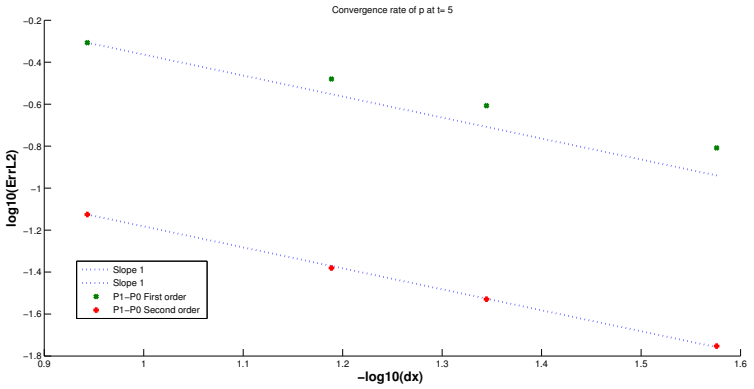

FIGURE 8. Convergence rate - Computation of the L_2-error of the solution p at time $t = 5s$ for the first and the second order scheme.

The idea is to initialize the simulation using the depth-averaged Euler model with the solitary wave of the Green-Naghdi model. Then, the aim is to compare after a long time lapse the analytical solution of the Green-Naghdi model and the simulated solution with the depth-averaged Euler model to see how the two models differ after a long time. We prescribe the amplitude $a = 0.2\,m$, the elevation $H_0 = 1.0\,m$ and the velocity $c_0 = 3.43\,m/s$ and, from (75), we deduce the values of l and d for the Green-Naghdi model.

Remark 4. The parameters c_0 and a have been chosen such that, if we compute the solitary solution of the depth-averaged Euler model (70)-(73) with the parameters (74), the two waves only slightly differ, as one can see in figure 9.

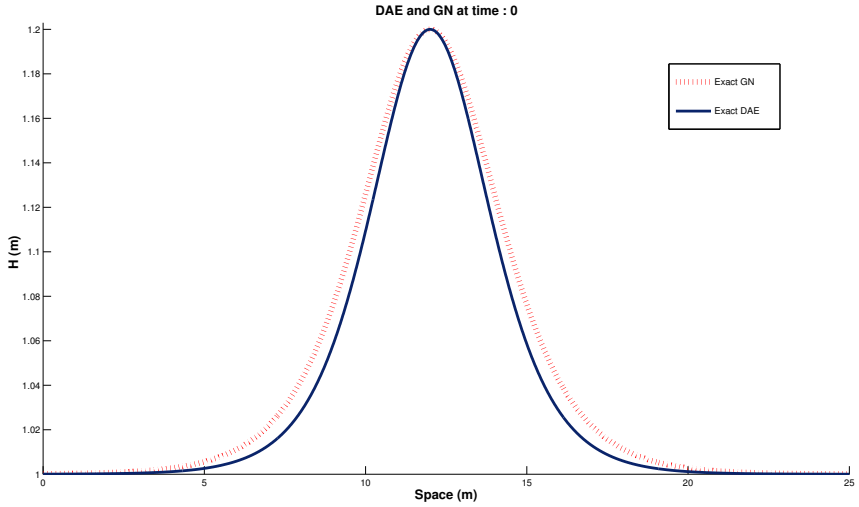

FIGURE 9. The solitary wave - Comparison of the two analytical solutions for the depth-averaged Euler system (DAE) and the Green-Naghdi model (GN) at time $t = 0$, for the same amplitude $a = 0.2\,m$ and the same velocity $c_0 = 3.43 m/s$.

In figure 10, the simulation in a long channel of $80\,m$ has been initialized with the solitary wave of the Green-Naghdi model. The elevation of the simulated wave is compared with the analytical solutions of the Green-Naghdi model at different times. There is a significant gap between the two curves after a long time lapse, showing the discrepancy between the solution of the two models.

Remark 5. Another unsteady solution has been presented in [13] and generalizes the solution obtained by Thacker [38] for the shallow water equation. Although it is not studied in this paper, in the same way as the solitary wave, notice that the solution can be adapted for the Green-Naghdi model.

5. Numerical results.

5.1. Dam break problem.

We next study the dispersive effect on the classical dam break problem, which is usually modeled by a Riemann problem providing

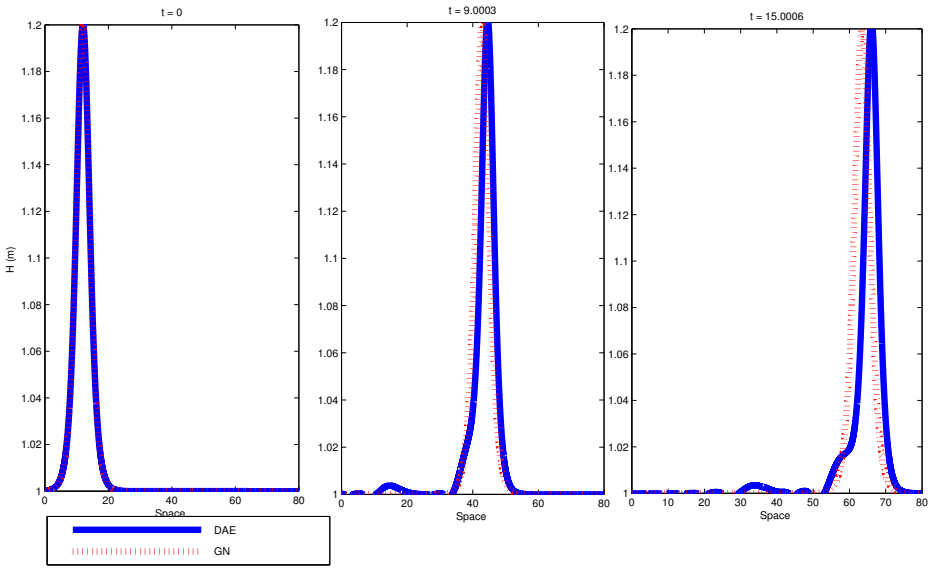

FIGURE 10. The solitary wave - Comparison of a DAE simulation with an analytical solution of the Green-Naghdi model at times : $t = 0\,s$, $t = 3.003\,s$, $t = 18.0008\,s$.

a left state (H_L, u_L) and a right state (H_R, u_R) on each side of the discontinuity x_d ([23]). However, our numerical dispersive model does not allow discontinuous solutions due to the functional spaces required for H (see also [13]), thus we provide an initial data numerically close to the analytical one

$$\begin{aligned} H(x,0) &= (H_R + a) - a \tanh\left(\frac{x - x_d}{\epsilon}\right), \\ a &= H_R - H_L. \end{aligned}$$

To evaluate the non hydrostatic effect, the different fields have been compared with the shallow water solution with the initial data: $H_L = 1.8\,m$, $H_R = 1\,m$, $u_R = u_L = 0\,m.s^{-1}$, $\epsilon = 10^{-4}\,m$, $x_d = 300\,m$ over a domain of length $600\,m$ with 30000 nodes. In figure 11, the evolution of the state is shown at time $t = 10\,s$ and $t = 45\,s$. The oscillations are due to the dispersive effects but the mean velocity does not change. These results are in adequation with the analysis proposed by Gavrilyuk in [30] for the Green-Naghdi model with the same configuration.

5.2. **Wet-dry interfaces.** The ability to treat the wet/dry interfaces is crucial in geophysical problems, since geophysicists are interested in studying the behavior of the water depth near the shorelines. This implies a water depth tending to zero at such boundaries. To treat the problem, we use the method introduced in [1], considering a minimum elevation H_ϵ.

Therefore, we confront the method with a coastal bottom at the right boundary over a domain of $35\,m$ with 3000 nodes. A wave is generated at the left boundary

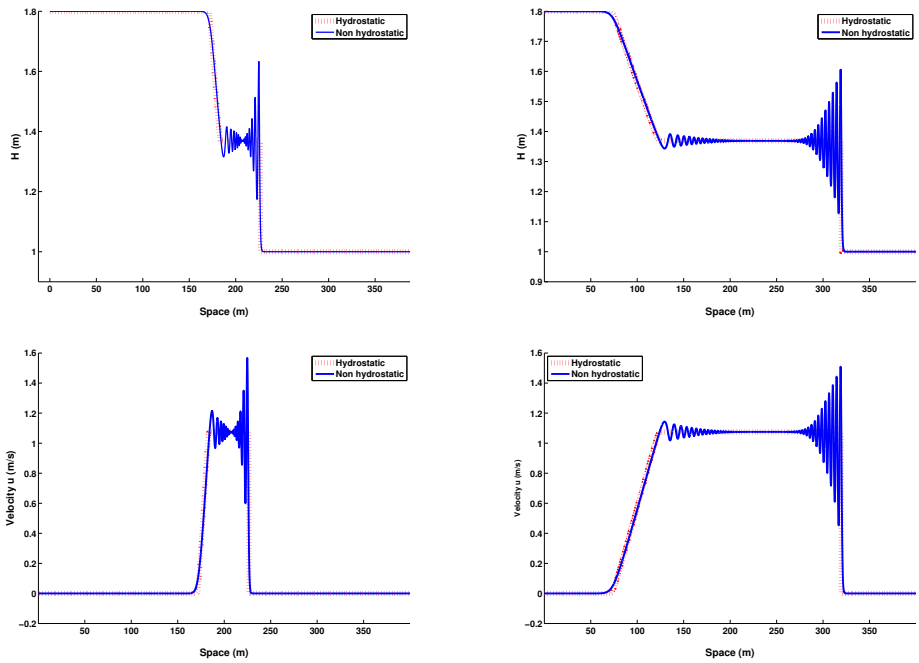

FIGURE 11. The dam break problem, elevation H and velocity u at times $t = 10\,s$ and $t = 45\,s$.

with an amplitude of $0.2\,m$ and an initial water depth $H_0 = 1\,m$. In figure 12, the arrival of the wave at the coast is shown for times $t = 7.91\,s$, $9.92\,s$ and $10.42\,s$.

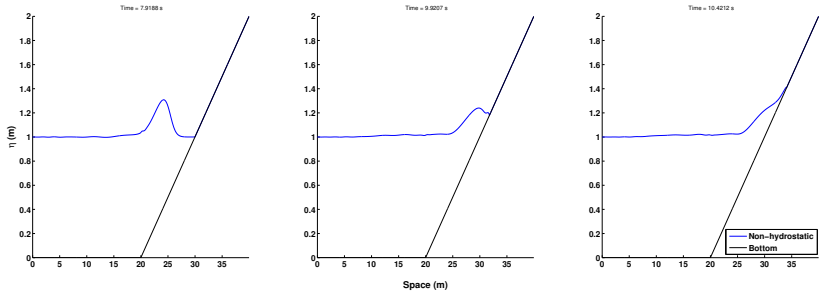

FIGURE 12. Propagation of a wave at a wet/dry interface.

5.3. **Comparison with experimental results.** In this part, we confront the model with Dingemans experiments (detailed in [19, 18]) that consist in generating a small amplitude wave at the left boundary of a channel with topography as described in figure 13.

At the left boundary, a wave is generated with a period $T = 2.02\,s$ and an amplitude of $0.02\,m$. A free outflow condition is set at the right boundary. The initial free surface is set to be $\eta_0 = 0.4\,m$, and the measurement readings are saved

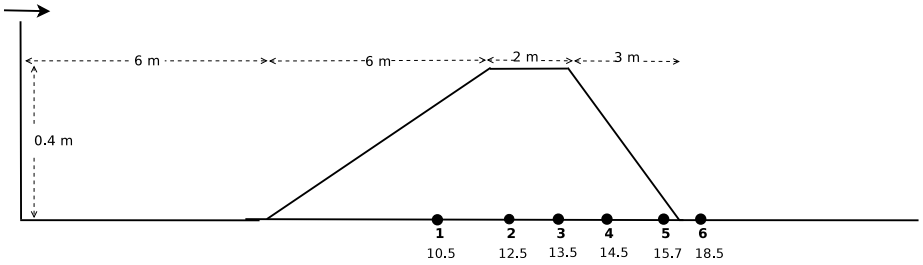

FIGURE 13. Configuration of Dingemans's test.

at the following positions $10.5\,m$, $12.5\,m$, $13.5\,m$, $14.5\,m$,$15,7\,m$ and $17.3\,m$, placed at sensors 1 to 6 (Fig.13). In such a situation, the non hydrostatic effects have a significant impact on the water depth that cannot be represented by a hydrostatic model. These effects result mainly from the slope of the bathymetry, 10% in this case. In the figure 14, the simulation has been run with the hydrostatic model and the elevation has been compared with measures at the sensor 5. As one can see, the non-hydrostatic pressure has to be taken in consideration to estimate the real water depth variation.

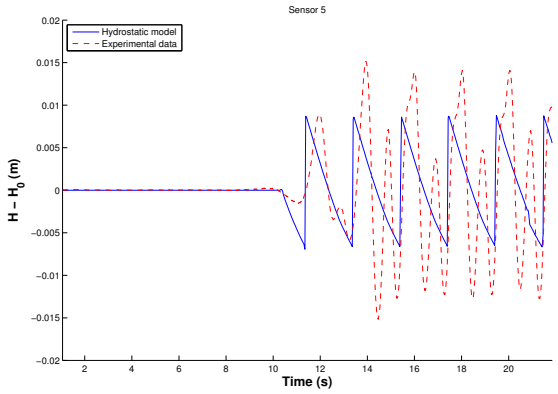

FIGURE 14. Comparison with hydrostatic model on sensor 5.

The numerical simulation with the non-hydrostatic model has been run with 15000 nodes on a domain of $49\,m$ over $25\,s$ and the comparisons are illustrated for each sensor (fig. 15). The goal of this last result is also to highlight the ability of the model to capture dispersive effects for a geophysical flow with a non negligible pressure.

Remark 6. The reader can refer to [16, 20] to see the numerical results of the Green-Naghdi model on the Dingemans test. As expected, for the two models, the numerical results are close to the experimental data. Notice that the measured quantities contain experimental errors and uncertainties. Therefore, since the two models are very close and the generated perturbation during the experiment is small, it is complicated to evaluate if the differences are due to the uncertainty of

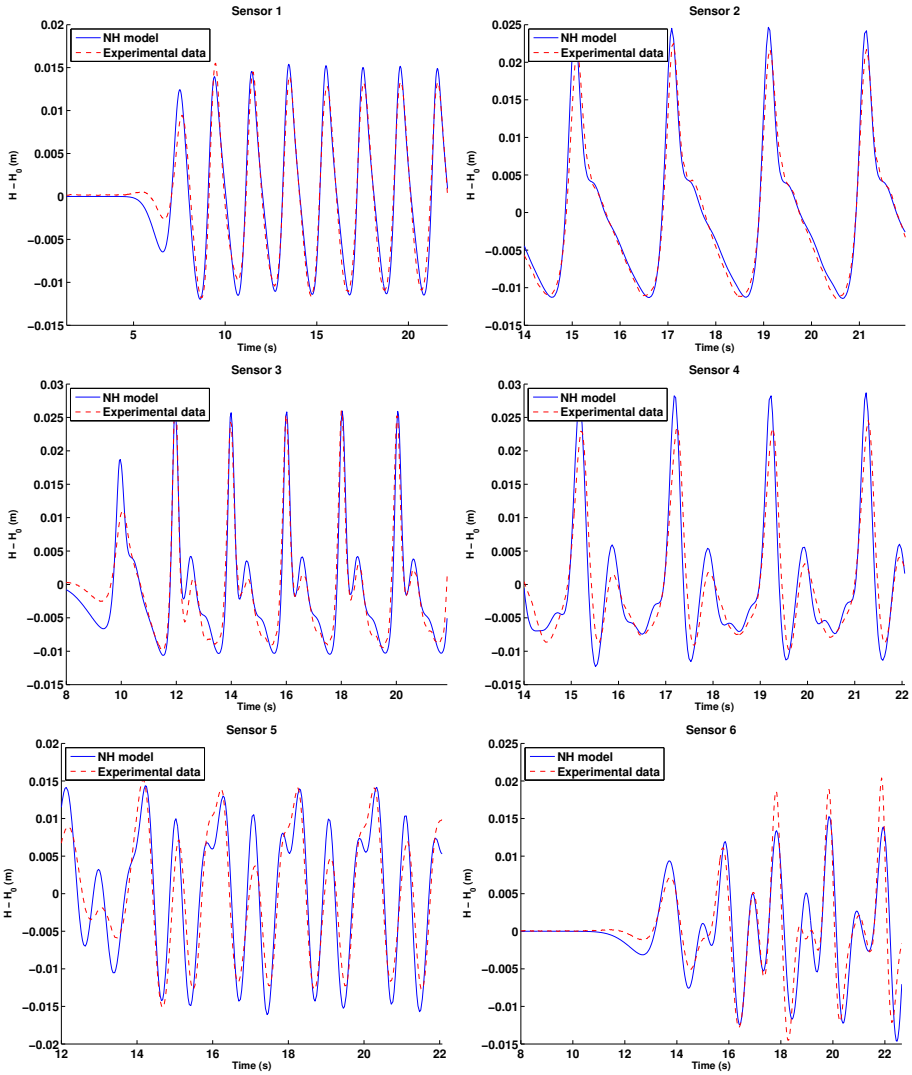

FIGURE 15. Comparison between measured and computed elevations on Dingemans test for the six first sensors.

the measures or the accuracy of the models. Nevertheless, it is expected that the difference between the models would be observable after a long time. Although this is not the scope of this paper, it would be interesting in a future study to compare the two models on the same experimental data.

5.4. **Remark on iterative method.** We recall that this formulation should allow to extend the method on two dimensional unstructured grids. However, it requires to invert a system at each time iteration, which will become too costly in two dimensions. To anticipate the two dimensional problem, this method has been tested using different iterative methods like conjugate gradient and Uzawa methods. In figure 16, we show a comparison of the computing time for the implementation of the direct method and Uzawa method for $\mathbb{P}_1$-iso-$\mathbb{P}_2/\mathbb{P}_1$ approximation. In one

dimension, it is not relevant to use one of these methods, while it will be necessary for the two dimension model.

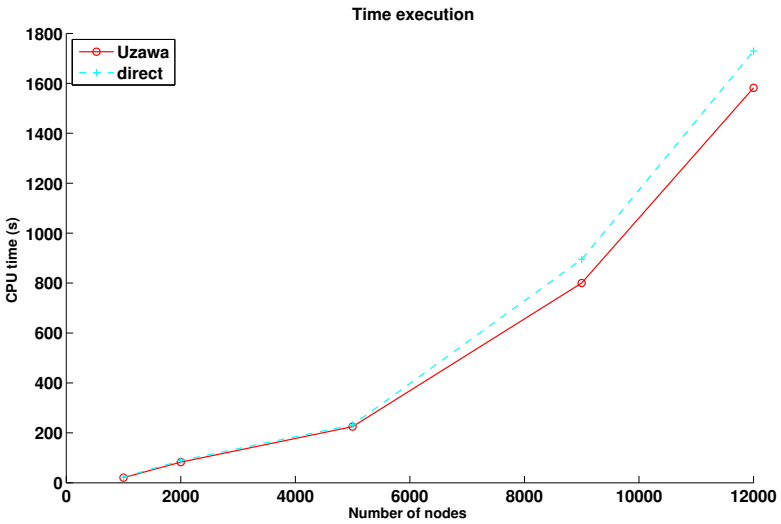

FIGURE 16. Comparison of the computing time (CPU) for the direct method and Uzawa method with $\mathbb{P}_1$-iso-$\mathbb{P}_2/\mathbb{P}_1$ approximation.

6. **Conclusion.** In this paper, a variational formulation has been established for the one dimensional dispersive model introduced in [13]. The main idea is to give a new framework in which it will be possible to extend the scheme to the two dimensional model. To this aim, the finite-element method has been presented with two approximation spaces. First, the $\mathbb{P}_1/\mathbb{P}_0$ approximation has been done and we recover, as expected, the finite difference scheme, together with the good results proved in [1]. Then, the $\mathbb{P}_1$-iso-$\mathbb{P}_2/\mathbb{P}_1$approximation has been studied to prepare the two dimensional problem. We have validated the method using several numerical tests and studying the dispersive effect on geophysical situations.

Acknowledgments. The authors acknowledge the Inria Project Lab Algae in Silicio for its financial support.

REFERENCES

[1] N. Aïssiouene, M. O. Bristeau, E. Godlewski and J. Sainte-Marie, A robust and stable numerical scheme for a depth-averaged Euler system, Submitted.

[2] B. Alvarez-Samaniego and D. Lannes, Large time existence for 3D water-waves and asymptotics, *Invent. Math.*, **171** (2008), 485–541.

[3] B. Alvarez-Samaniego and D. Lannes, A Nash-Moser theorem for singular evolution equations. Application to the Serre and Green-Naghdi equations, *Indiana Univ. Math. J.*, **57** (2008), 97–131.

[4] E. Audusse, F. Bouchut, M.-O. Bristeau, R. Klein and B. Perthame, A fast and stable well-balanced scheme with hydrostatic reconstruction for Shallow Water flows, *SIAM J. Sci. Comput.*, **25** (2004), 2050–2065.

[5] E. Audusse, F. Bouchut, M.-O. Bristeau and J. Sainte-Marie, Kinetic entropy inequality and hydrostatic reconstruction scheme for the Saint-Venant system., 2014, URL http://hal.inria.fr/hal-01063577, (Submitted) http://hal.inria.fr/hal-01063577/PDF/kin_hydrost.pdf.

[6] J.-L. Bona, T.-B. Benjamin and J.-J. Mahony, Model equations for long waves in nonlinear dispersive systems, *Philos. Trans. Royal Soc. London Series A*, **272** (1972), 47–78.

[7] P. Bonneton, E. Barthelemy, F. Chazel, R. Cienfuegos, D. Lannes, F. Marche and M. Tissier, Recent advances in Serre-Green Naghdi modelling for wave transformation, breaking and runup processes, *European Journal of Mechanics - B/Fluids*, **30** (2011), 589–597, URL http://www.sciencedirect.com/science/article/pii/S0997754611000185, Special Issue: Nearshore Hydrodynamics.

[8] F. Bouchut, An introduction to finite volume methods for hyperbolic conservation laws, *ESAIM Proc.*, **15** (2005), 1–17.

[9] F. Bouchut, *Nonlinear Stability of Finite Volume Methods for Hyperbolic Conservation Laws and Well-Balanced Schemes for Sources*, Birkhäuser, 2004.

[10] F. Brezzi, On the existence, uniqueness and approximation of saddle-point problems arising from Lagrangian multipliers, *Rev. Française Automat. Informat. Recherche Opérationnelle Sér. Rouge*, **8** (1974), 129–151.

[11] M.-O. Bristeau and B. Coussin, *Boundary Conditions for the Shallow Water Equations Solved by Kinetic Schemes*, Rapport de recherche RR-4282, INRIA, 2001, URL http://hal.inria.fr/inria-00072305, Projet M3N.

[12] M.-O. Bristeau, N. Goutal and J. Sainte-Marie, Numerical simulations of a non-hydrostatic Shallow Water model, *Computers & Fluids*, **47** (2011), 51–64.

[13] M. O. Bristeau, A. Mangeney, J. Sainte-Marie and N. Seguin, An energy-consistent depth-averaged Euler system: Derivation and properties, *Discrete Contin. Dyn. Syst. Ser. B*, **20** (2015), 961–988, URL http://aimsciences.org/journals/displayArticlesnew.jsp?paperID=10801.

[14] M.-O. Bristeau and J. Sainte-Marie, Derivation of a non-hydrostatic shallow water model; Comparison with Saint-Venant and Boussinesq systems, *Discrete Contin. Dyn. Syst. Ser. B*, **10** (2008), 733–759.

[15] R. Camassa, D. Holm and J. Hyman, A new integrable shallow water equation, *Adv. Appl. Math.*, **31** (1994), 1–33.

[16] F. Chazel, D. Lannes and F. Marche, Numerical simulation of strongly nonlinear and dispersive waves using a Green–Naghdi model, *J. Sci. Comput.*, **48** (2011), 105–116.

[17] A. J. Chorin, Numerical solution of the Navier-Stokes equations, *Math. Comp.*, **22** (1968), 745–762.

[18] M.-W. Dingemans, *Wave Propagation Over Uneven Bottoms*, Advanced Series on Ocean Engineering - World Scientific, 1997.

[19] M. Dingemans, *Comparison of Computations with Boussinesq-like Models and Laboratory Measurements*, Technical Report H1684-12, AST G8M Coastal Morphodybamics Research Programme, 1994.

[20] A. Duran and F. Marche, Discontinuous-Galerkin discretization of a new class of Green-Naghdi equations, *Communications in Computational Physics*, **17** (2015), 721–760, URL https://hal.archives-ouvertes.fr/hal-00980826.

[21] W. E and J.-G. Liu, Projection method I: Convergence and numerical boundary layers, *SIAM J. Numer. Anal.*, **32** (1995), 1017–1057.

[22] A. Ern and S. Meunier, A posteriori error analysis of euler-galerkin approximations to coupled elliptic-parabolic problems, *ESAIM Math. Model. Numer. Anal.*, **43** (2009), 353–375, URL http://journals.cambridge.org/abstract_S0764583X05000166.

[23] E. Godlewski and P.-A. Raviart, *Numerical Approximations of Hyperbolic Systems of Conservation Laws*, Applied Mathematical Sciences, vol. 118, Springer, New York, 1996.

[24] A. Green and P. Naghdi, A derivation of equations for wave propagation in water of variable depth, *J. Fluid Mech.*, **78** (1976), 237–246.

[25] P. Gresho and S. Chan, Semi-consistent mass matrix techniques for solving the incompressible Navier-Stokes equations, *First Int. Conf. on Comput. Methods in Flow Analysis*, Okayama University, Japan.

[26] J.-L. Guermond, Some implementations of projection methods for Navier-Stokes equations, *ESAIM: Mathematical Modelling and Numerical Analysis*, **30** (1996), 637–667, URL http://eudml.org/doc/193818.

[27] J.-L. Guermond and J. Shen, On the error estimates for the rotational pressure-correction projection methods, *Math. Comput.*, **73** (2004), 1719–1737, URL http://dblp.uni-trier.de/db/journals/moc/moc73.html#GuermondS04.

[28] H. Johnston and J.-G. Liu, Accurate, stable and efficient Navier-Stokes solvers based on explicit treatment of the pressure term, *Journal of Computational Physics*, **199** (2004), 221–259, URL http://www.sciencedirect.com/science/article/pii/S002199910400083X.
[29] D. Lannes and P. Bonneton, Derivation of asymptotic two-dimensional time-dependent equations for surface water wave propagation, *Physics of Fluids*, **21** (2009), 016601.
[30] O. Le Métayer, S. Gavrilyuk and S. Hank, A numerical scheme for the Green-Naghdi model, *J. Comput. Phys.*, **229** (2010), 2034–2045.
[31] R.-J. LeVeque, *Finite Volume Methods for Hyperbolic Problems*, Cambridge University Press, 2002.
[32] O. Nwogu, Alternative form of Boussinesq equations for nearshore wave propagation, *Journal of Waterway, Port, Coastal and Ocean Engineering, ASCE*, **119** (1993), 618–638.
[33] D. Peregrine, Long waves on a beach, *J. Fluid Mech.*, **27** (1967), 815–827.
[34] O. Pironneau, *Méthodes Des Éléments Finis Pour Les Fluides.*, Masson, 1988.
[35] R. Rannacher, On Chorin's projection method for the incompressible Navier-Stokes equations, in *The Navier-Stokes Equations II – Theory and Numerical Methods* (eds. G. Heywood John, K. Masuda, R. Rautmann and A. Solonnikov Vsevolod), vol. 1530 of Lecture Notes in Mathematics, Springer Berlin Heidelberg, 1992, 167–183, URL http://dx.doi.org/10.1007/BFb0090341.
[36] J. Shen, Pseudo-compressibility methods for the unsteady incompressible Navier-Stokes equations, *11th AIAA Computational Fluid Dynamic Conference*, Orlando, FL, USA.
[37] J. Shen, On error estimates of the penalty method for unsteady Navier-Stokes equations, *SIAM J. Numer. Anal.*, **32** (1995), 386–403.
[38] W. C. Thacker, Some exact solutions to the non-linear shallow water wave equations, *J. Fluid Mech.*, **107** (1981), 499–508.

Received June 2015; revised October 2015.

E-mail address: Nora.Aissiouene@inria.fr
E-mail address: Marie-Odile.Bristeau@inria.fr
E-mail address: Edwige.Godlewski@upmc.fr
E-mail address: Jacques.Sainte-Marie@inria.fr